



Kay Raum and Pascal Laugier

Abstract

Although it has been over 30 years since the first recorded use of quantitative ultrasound (QUS) technology to predict bone strength, the field has not yet reached its maturity. Among several QUS technologies available to measure cortical or cancellous bone sites, at least some of them have demonstrated potential to predict fracture risk with an equivalent efficiency compared to X-ray densitometry techniques, and the advantages of being non-ionizing, inexpensive, portable, highly acceptable to patients and repeatable. In this Chapter, we review instrumental developments that have led to in vivo applications of bone QUS, emphasizing the developments occurred in the decade 2010–2020. While several proposals have been made for practical clinical use, there are various critical issues that still need to be addressed, such as quality control and standardization. On the other

side, although still at an early stage of development, recent QUS approaches to assess bone quality factors seem promising. These include guided waves to assess mechanical and structural properties of long cortical bones or new QUS technologies adapted to measure the major fracture sites (hip and spine). New data acquisition and signal processing procedures are prone to reveal bone properties beyond bone mineral quantity and to provide a more accurate assessment of bone strength.

Keywords

Attenuation · Axial transmission · Cortical bone · Trabecular bone · Speed of sound · Transverse transmission

K. Raum (✉)

Charité—Universitätsmedizin Berlin, Corporate Member of Freie Universität Berlin, Humboldt-Universität zu Berlin, CC04 Center for Biomedicine, Berlin, Germany
e-mail: kay.raum@charite.de

P. Laugier

Sorbonne Université, INSERM, CNRS, Laboratoire d'Imagerie Biomédicale, Paris, France
e-mail: laugierp@gmail.com

3.1 Introduction

The current established standard method for the in-vivo assessment of bone strength and of its clinical counterpart, the risk of fracture, is based on the measurement of bone mineral density (BMD) by means of dual-energy X-ray absorptiometry (DXA) (Miller et al., 2002). While BMD is an important predictor of bone strength (Bouxsein et al., 1999), additional

factors are required to explain individual strength more accurately. These include tissue-intrinsic structural and viscoelastic material properties. Because ultrasound wave propagation is governed by the structural and material properties of the propagation medium, a diversity of innovative technological developments targeting the in-vivo characterization of bone strength has been implemented in medical devices (Table 3.1). The first clinical application of ultrasound waves to bone, using propagation in cortical bone, was described in the late 1950s for monitoring fracture healing at the tibia (Siegel et al., 1958). The technique did not have a great success. It was revived 30 years later by Alexej Tatarinov and colleagues to assess bone conditions during bed rest studies conducted to simulate long exposure to weightlessness. These studies published in Russian have gone unnoticed in the West but marked the beginning of axial transmission techniques dedicated to the measurement of guided waves in cortical bone. Investigations on the field are still going on as detailed later in this Chapter and also in Chaps. 4 and 5 of this book.

The introduction of quantitative ultrasound (QUS) methods in the field of osteoporosis followed the study published in 1984 by Langton et al. (1984), a seminal work that strongly influenced later developments, demonstrating that the slope of the frequency-dependent attenuation at the calcaneus could discriminate osteoporotic from non-osteoporotic patients. This led to the opening of a new research and development area known as bone QUS.

Many advances have been achieved during the last 30 years and a variety of technologies have been introduced to assess in vivo the skeletal status by providing measurements of ultrasonic parameters of cancellous bone or cortical bone at multiple anatomical sites, e.g., calcaneus, fingers phalanges, radius, tibia, proximal femur, and spine (Fig. 3.1). Theoretical and numerical studies emerged, and several different techniques were tested with more or less success. These include backscattering,

propagation in poroelastic media, guided waves, and pulse-echo imaging. By coupling model to experimental data, these approaches have the power to derive bone biomarkers that reflect structural and material properties. Research is continuing in most of these areas.

The absence of exposure to ionizing radiation, the portability and the modest cost of the machines are appealing factors of QUS devices. The main clinical field of application is fracture risk prediction for osteoporosis (see Chap. 2), although many other pathological bone conditions may benefit from ultrasound measurements, e.g., monitoring of fracture healing (Nicholson et al., 2020), monitoring of implant osseointegration (see Chap. 17), assessment of spinal deformities (Lam et al., 2011; Wong et al., 2019) (see Chap. 16), as a treatment monitoring tool for the management of rare bone diseases in children (Raimann et al., 2020), assessment of skeletal status in neonates and infants (Liu et al., 2020; Mao et al., 2019), and for the screening of adolescents and young adults (Jafri et al., 2020).

As described in Chap. 2, the clinical validation for fracture risk prediction and the acceptance among clinicians is however not identical for all devices (Njeh et al., 2000). Until now, only heel QUS measures are proven to predict hip fractures and all osteoporotic fractures with similar relative risk as other central X-ray based bone density measurements (Gluer et al., 2004; Krieg et al., 2008; Marin et al., 2006; Moayyeri et al., 2009) (see Chap. 2). This Chapter describes the different clinical devices that have been developed for the in-vivo assessment of skeletal status in the context of the clinical management of osteoporosis. They can be classified according to the targeted tissue type (trabecular vs. cortical bone), measurement type (axial vs. transverse transmission, pulse-echo), and the type of interaction of the acoustic waves with the bone tissue (bulk compression/shear wave propagation, guided wave propagation, single vs. multi-path propagation, specular reflection vs. scattering). Depending on the type of measurement, different acoustic fre-

Table 3.1 Overview of clinical bone QUS devices covered in this Chapter and respective vendors, measurement sites, and measurement parameters. The last columns provide references, from which information was compiled

Device	Vendor	Measurement site	Measurement parameter	References
Trabecular transverse transmission (Tr.TT)				
Achilles	GE Lunar, Madison, WI, USA	Calcaneus	BUA, SOS, SI	Dobnig et al. (2007), Gluer et al. (2004), Gonnelli et al. (2005), Njeh et al. (2000) and Ramteke et al. (2017)
Sahara	Hologic	Calcaneus	BUA, QUI	Delshad et al. (2020), Gluer et al. (2004), He et al. (2000), Miller et al. (2002), Olmos et al. (2020) and To and Wong (2011)
UBIS	Diagnostic Medical Systems, Montpellier, France	Calcaneus	BUA, SOS	Gluer et al. (2004) and Sasagawa et al., (2011)
DTU	Meditech, Hawthorn, CA, USA	Calcaneus	BUA, SOS	Gluer et al. (2004)
CUBA	McCue Ultrasonics, Winchester, UK	Calcaneus	BUA	Chan et al. (2013)
AOS-100	Hitachi Medical Systems, Singapore	Calcaneus	SOS, TI, OSI	Njeh et al. (2000) and Tsuda-Futami et al. (1999)
Sonost	Osteosys Corp., Seoul, Korea	Calcaneus	BUA, SOS, BQI	Jafrri et al. (2020)
Cortical transverse transmission (Ct.TT)				
DBM Sonic Bone Profiler	IGEA, Carpi, Italy	Finger phalanx	AD-SOS, BTT, UBPS	Gluer et al. (2004), Gonnelli et al. (2005), Sakata et al. (2004) and Savino et al. (2013)
LD-100	OYO Electric Co., Ltd. Kyoto, Japan	Radius	Attenuation, Radius Thickness, CT.Th, Trabecular Prop, Elasticity	Breban et al. (2010)
Ultrascan	CyberLogic, Inc., New York, NY, USA	Radius	NTD _{cw} , NTD _{Dw}	Stein et al. (2013)

(continued)

Table 3.1 (continued)

Device	Vendor	Measurement site	Measurement parameter	References
Cortical axial transmission (CLAT)				
Soundscan	Myriad, Myriad Ultrasound Systems Ltd., Israel	Tibia	SOS	Foldes et al. (1995)
Omniscense	Sunlight ultrasound Technologies Ltd., Rehovot, Israel	Distal radius Tibia Proximal phalanx	SOS	Dobnig et al. (2007), Roggen et al. (2015) and Shenoy et al. (2017)
Sono	Oscare Medical Oy, Vantaa, Finland	Distal radius Tibia	SOS	Moiilanen et al. (2013)
BDAT	Azalée, Paris, France	Distal radius Tibia	Ct.Th _{US} Ct.Po _{US}	Minonzio et al. (2019) and Schneider et al. (2019)
Cortical pulse-echo (Ct.PE)				
BI	Bone Index Finland Ltd, Kuopio, Finland	Distal radius Proximal tibia Distal tibia	Ct.Th _{APP} DI	Behrens et al. (2016), Karjalainen et al. (2008), Karjalainen et al. (2012), Lewiecki (2020), Nazari-Farsani et al. (2020), Schousboe et al. (2017) and van den Berg et al. (2020)
Trabeculae pulse-echo (Tr.PE)				
Echo	Echolight Spa, Lecce, Italy	Femoral neck Lumbar spine	BMD _{US} T-score Z-score FS	Adami et al. (2020), Casciaro et al. (2016), Di Paola et al. (2019) and Diez-Perez et al. (2019)

AD-SOS Amplitude-Dependent Speed of Sound, *BMD_{US}* Ultrasound derived BMD value, *BTT* Bone Transmission Time, *BUA* Broadband Ultrasound Attenuation, *BQI* Bone Quality index, *CT.Th* Cortical Thickness (the subscripts US and APP denote real ultrasound based thickness and apparent thickness), *FS* Fragility Score, *NTD* Net Time Delay (the subscripts CW and DW denote circumferential and direct waves, respectively), *DI* Density Index, *OSI* Osteo-Sono-assessment Index, *SOS* Speed Of Sound, *SI* Stiffness Index, *QUI* Quantitative Ultrasound Index, *UBPS* Ultrasound Bone Profile Score, *TI* Transmission Index

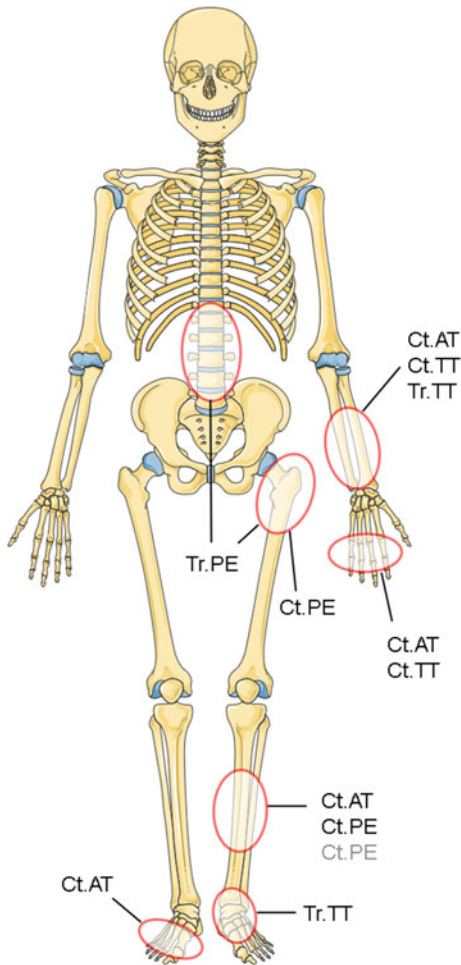


Fig. 3.1 Overview of different measurement locations of clinical QUS devices (Adapted from Servier Medical Art by Servier under a Creative Commons Attribution 3.0 Unported License). See Table 3.1 for the explanation of the abbreviations and a summary of the clinical devices used at the indicated anatomical measurement sites

quency ranges and transmitter/receiver arrangements are used, and a plethora of acoustical, structural, elastic, and surrogate properties are derived. While most clinical bone QUS devices aim at deriving a BMD surrogate parameter based on empirically derived correlations with the DXA-based BMD reference, some recent devices provide quantitative structural bone biomarkers, e.g., cortical thickness and porosity, which are known to be related to bone strength (Iori et al., 2020) and fracture risk (Bala et al., 2014; Bjornerem et al., 2013). In the present Chapter, the most

important clinical bone QUS devices (Table 3.1) are classified and presented according to their measurement principle, i.e.,

- Trabecular transverse transmission (Tr.TT)
- Cortical transverse transmission (Ct.TT)
- Cortical axial transmission (Ct.AT)
- Cortical pulse-echo (Ct.PE)
- Trabecular pulse-echo (Tr.PE)

Some devices introduced in the Chapter are also described in detail in other Chapters of this book. A short description of the basic principles will be given here and we refer our readers to the corresponding Chapters for a comprehensive technical and performance description of these devices. Recent techniques, such as pulse-echo imaging (Chaps. 9 and 10) and tomography (Chap. 11) not implemented yet in clinical devices, are not covered by the present Chapter, but the readership will find more information in the corresponding Chapters of this book.

3.2 Trabecular Transverse Transmission (Tr.TT)

The transverse transmission technique uses transmitter and receiver placed on opposite sides of the skeletal site to be measured. Systems with single-element focused transducer pairs coupled to a mechanical scanning device as well as array systems have been developed. While the calcaneus (heel bone) is the preferred skeletal site, the method has also been applied at the proximal femur at the hip (Barkmann et al., 2008, 2010). Principles of measurements have been detailed in (Chappard et al., 1997; Laugier et al., 1997) and are only briefly recalled here for the sake of completeness.

Assuming that the system response and the propagation are linear, the propagation characteristics such as attenuation and velocity are obtained using the well-known substitution technique, i.e., the signal transmitted through the skeletal site in response to a broadband ultrasonic excitation is compared to the signal transmitted through a reference medium such as water of known attenuation. The frequency-dependent

attenuation is obtained from the spectral analysis of the two signals $A^{ref}(f)$ and $A(f)$, typically using a Fast Fourier Transform algorithm.

3.2.1 Broadband Ultrasound Attenuation (BUA)

The apparent frequency-dependent attenuation, i.e., the signal loss, is defined on a logarithmic scale as follows:

$$\hat{\alpha}(f) l = \ln \frac{|A^{ref}(f)|}{|A(f)|} \quad (3.1)$$

where $\hat{\alpha}(f)$ is the measured apparent attenuation coefficient. In the frequency range used to make in-vivo measurements of the human calcaneus, the ultrasonic attenuation varies quasi-linearly with frequency (Chaffai et al., 2000; Wear, 2001). Therefore, the slope of a linear regression fit to $\hat{\alpha}(f) \cdot l$ in the frequency range of approximately 0.2–0.6 MHz yields the BUA value. The extraction of an unbiased attenuation slope from the empirically determined signal loss in Eq. 3.1 assumes that (i) the effect of diffraction is small and can be neglected (Droin et al., 1998; Xu and Kaufman, 1993), (ii) transmission losses are independent of frequency (the effect of interface losses on the attenuation curve is a simple vertical offset which does not affect the slope estimate) (Strelitzki and Evans, 1998) and (iii) phase cancellation effects are negligible, which is the case if the sample thickness and speed of sound across the ultrasonic beam profile are uniform. Overlapping of fast and slow waves (see Chap. 6) may also cause phase cancellation (Anderson et al., 2008; Bauer et al., 2008) but is usually not a concern for in vivo measurements, at least at the heel. The measurements yield the total loss through the intervening tissues in the beam, i.e., bone and surrounding soft tissues. The effect of the latter is generally neglected (Laugier, 2008). Not many devices do provide an estimate of the bone thickness. Therefore, the slope of the frequency-dependent attenuation (BUA) rather than the slope of the attenuation coefficient (i.e., BUA normalized by thickness) is measured.

The Hitachi AOS-100 does not perform a spectral analysis to measure BUA. Instead, the signal is analyzed in the time-domain and the ‘‘Transmission Index’’ TI, defined as the full-width-half-maximum of the first positive peak of the received waveform is measured instead (Tsuda-Futami et al., 1999).

3.2.2 Speed of Sound

Two principal approaches have been used to measure SOS. The first one assumes that c is frequency-independent and uses simple time-domain methods, i.e., c is simply calculated from the difference of two time-of-flight (TOF) measurements, whereas for the first and second measurements the signal is transmitted through the reference material alone and through the reference material and the heel, respectively:

$$\begin{aligned} \text{reference material : } TOF^{ref} &= \frac{L}{c_{ref}} \\ \text{reference material and sample : } & \\ TOF &= \frac{L-l}{c_{ref}} + \frac{l}{c} \\ \text{difference signal : } \Delta TOF &= \frac{l}{c} - \frac{l}{c_{ref}} \end{aligned} \quad (3.2)$$

$$c = \frac{1}{\frac{1}{c_{ref}} + \frac{\Delta TOF}{l}} \quad (3.3)$$

If measurements are taken using probes in direct contact to the skin equation Eq. 3.3 reduces to:

$$c = \frac{l}{TOF} \quad (3.4)$$

Various criteria are used to estimate TOF, for example the first arrival point, the first zero-crossing point, or a fixed threshold on the rising front of the received electrical signal. However, frequency-dependent attenuation and velocity dispersion are acknowledged sources of bias when measuring velocity in the time domain (Droin et al., 1998; Nicholson et al., 1996; Strelitzki et al., 1996; Wear, 2000).

Because there is no consensus on a standardized protocol for velocity determinations in bone, the comparison or pooling of measurements obtained from different devices is particularly difficult. Wear has suggested a numerical method to compute corrections for previously acquired SOS, to improve standardization in bone sonometry and to overcome discrepancies in SOS estimates due to transit-time marker location (Wear, 2008), but such a method has not been implemented yet in practice. As discussed for BUA, the thickness l of the skeletal site must be known, and the impact of soft tissue must be neglected.

In the second approach, a frequency-dependent $c(f)$ is estimated from the phase $\varphi(f)$ of the complex ratio of the spectra:

$$\begin{aligned}\varphi(f) &= \text{atan} \left[\frac{A(f)}{A^{\text{ref}}(f)} \right] \\ &= 2\pi l f \left(\frac{1}{c_{\text{ref}}} - \frac{1}{c(f)} \right)\end{aligned}\quad (3.5)$$

After unwrapping the measured phase $\varphi(f)$, the phase velocity can be calculated as follows:

$$c(f) = \frac{1}{\frac{1}{c_{\text{ref}}} - \frac{\varphi_u(f)}{2\pi f l}} \quad (3.6)$$

where $\varphi_u(f)$ is the unwrapped phase.

3.2.3 Bone Stiffness and Quality Surrogates

The trabecular transverse transmission technique does not provide any direct measurement of stiffness, strength, or tissue quality. However, various surrogate parameters have been established (see Table 3.1.). The Lunar Achilles series provide a “Stiffness Index” SI, which is derived from normalized BUA and SOS values (Hans et al., 1994):

$$\begin{aligned}\text{SI} &= (\text{nBUA} + \text{nSOS}) / 2, \\ \text{nBUA} &= (\text{BUA} - 50) / 75 \times 100\% \\ \text{nSOS} &= (\text{SOS} - 1380) / 180 \times 100\%.\end{aligned}\quad (3.7)$$

Similarly, the Hologic Sahara provides the “Quantitative Ultrasound Index” QUI:

$$\text{QUI} = 0.41 \times (\text{SOS} + \text{BUA}) - 571. \quad (3.8)$$

SI and QUI values agree fairly well ($R = 0.83$, $p < 0.01$) (Alenfeld et al., 2002), but QUI values were found on average 2.4% higher than SI values, and the difference was more pronounced for higher ultrasound values (Ingle et al., 2001). The Hitachi AOS-100 combines SOS with the attenuation surrogate TI to an “Osteo Sono-Assessment Index” OSI as follows (Tsuda-Futami et al., 1999):

$$\text{OSI} = \text{TI} \times \text{SOS}^2. \quad (3.9)$$

These system-specific differences prevented a broader use of these parameters in clinical practice.

3.3 Cortical Transverse Transmission

The transducer configuration for cortical transverse transmission devices is similar to that of trabecular transverse transmission devices, but they have been introduced to measure the propagation of sound waves through both the cortical shell and medullary cavity. The DBM Sonic Bone Profiler measures the amplitude-dependent speed of sound (Ad-SOS) at the distal metaphysis of the first phalanx of fingers I–IV. The instrument is equipped with two 12-mm diameter, 1.25-MHz plane transducers mounted on an electronic caliper that measures the distance between the probes. The probes are positioned on the mediolateral surfaces of the distal metaphysis of the phalanx using the phalanx condyle as reference point. Coupling is achieved with a standard ultrasound gel. The probe positioning is slightly varied until the optimum signal (defined in terms of number of peaks and the amplitude of the peaks, following manufacturer recommendations) is recorded, then Ad-SOS is measured.

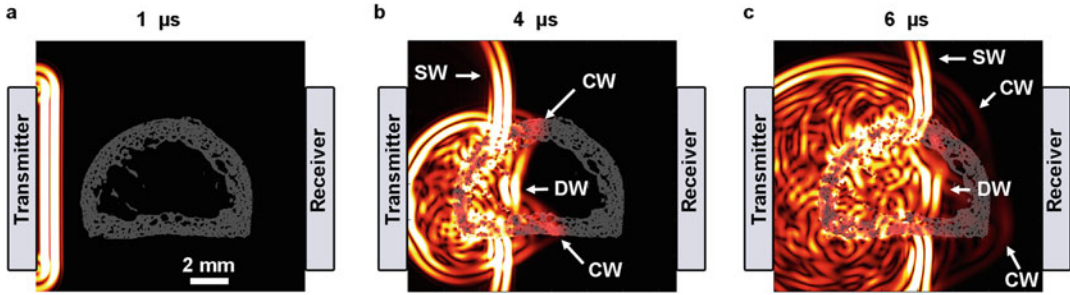


Fig. 3.2 Numerical sound propagation simulation (Bossy et al., 2002) through a human phalanx. A plane wave is transmitted from an unfocused transducer (a). Three distinct sound propagation pathways can be observed (b). Some waves bypass the bone and propagate through soft

tissue only (SW). Other waves either pass directly through cortical bone and the medullary cavity (DW) or are guided as circumferential waves (CW) within the cortical bone shell. Due to different propagation path lengths, the two circumferential waves reach the receiver at different travel times (c)

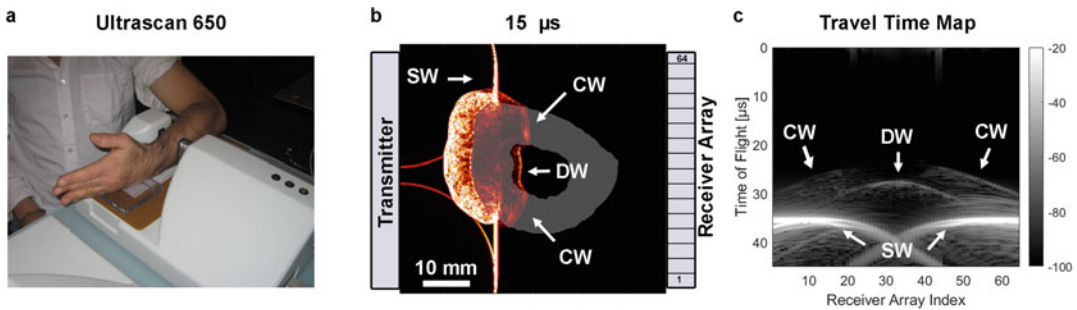


Fig. 3.3 The UltraScan 650 ultrasound bone assessment device (a) Numerical sound propagation simulation (Bossy et al., 2002) through a human radius showing three propagation paths. i.e., SW: soft tissue only; CW: cir-

cumferential wave; DW: direct wave (b) The 64-element receiver array allows a distinct analysis of the travel times of the SW, DW and CW signals. (a) and (b) were taken and adapted from Stein et al. (2013) with permission

Time-Of-Flight (TOF) is defined as the time between the emitted pulse and the first part of the signal that is above a predetermined amplitude threshold. The velocity measured with this technique is amplitude related and has been termed amplitude-dependent speed of sound (Ad-SOS). With this configuration, the fast waves (FW) are circumferential waves guided through the cortical shell (Fig. 3.2). In osteoporotic bones the attenuation is considerably higher than in normal bones and the amplitude of the first peak is too small to trigger the read-out electronics. The detection of the second peak is associated with an apparent longer travel time of flight. However, the exact propagation path length is unknown. Therefore, using the finger thickness rather than the exact path length results in an apparent speed of sound rather than in an accurate velocity estimate.

More recent systems apply the transverse transmission approach at the distal radius at the forearm. The Cyberlogic UltraScan (Fig. 3.3) consists of a rectangular single-element 3.5-MHz source transducer and a 1×4.8 cm 64-element receiver array (Stein et al., 2013). The radius is positioned at 1/3 location in the device. Similar to the phalanx configuration, three different sound propagation pathways can be distinguished. One “Direct Wave” (DW) travels through cortical bone and the medullary cavity. The “Circumferential Wave” (CW) is guided through the cortical shell. At the peripheral ends of the emitter-receiver pair, waves travelling through soft tissue only (SW) can be observed. The advantage of the array-receiver configuration is that the distinct travel times can be analyzed more easily. The device measures two ultrasound

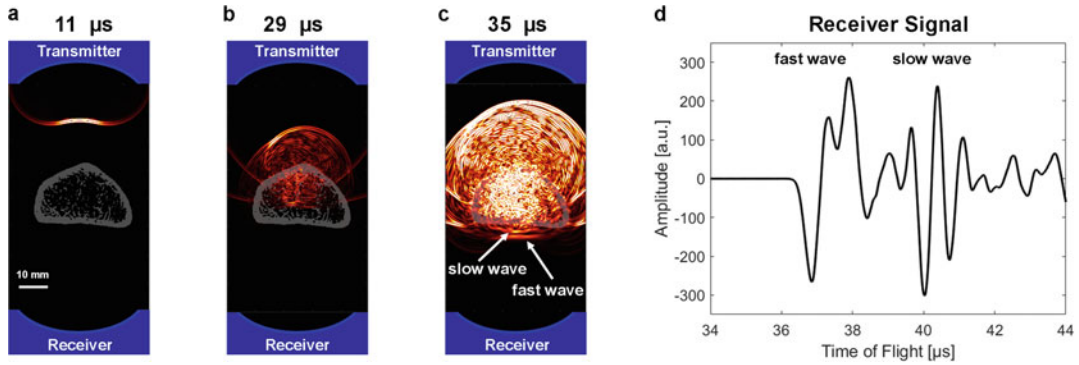


Fig. 3.4 Numerical sound propagation simulations (Bossy et al., 2002) of a focused wave through a human radius at three different time point showing the development of slow and fast waves (a–c), which

are recorded by the receiver (d). The travel-times and amplitudes of these waves are used to estimate apparent cancellous bone properties. The radius image was taken from Kazakia et al. (2013) with permission

net time delay (NTD) parameters: NTD_{DW} and NTD_{CW} define the difference between the transit times of waves traveling the DW and CW paths, respectively, and the travel time of the SW path. It has been shown in vitro that the cortical cross-sectional area CSA can be estimated by a non-linear combination of NTD_{DW} and NTD_{CW} ($R = 0.95$) (Le Floch et al., 2008):

$$CSA = a \times NTD_{CW} \times NTD_{DW} - b \times NTD_{DW}^2 + c. \quad (3.10)$$

A similar equation has been derived empirically in a clinical study on 60 adult subjects of both gender, age range between 22 and 84 years, to predict BMD values assessed at the same radius location ($R = 0.93$) (Stein et al., 2013):

$$BMD_{US} = 0.19 \times (NTD_{CW} \times NTD_{DW})^{1/2} + 0.28. \quad (3.11)$$

The LD-100 device (OYO Electrics, Kyoto, Japan, see Chap. 6, Fig. 6.13) is a hybrid technology, which combines transverse transmission measurements through cortical and trabecular bone compartments with pulse-echo measurements in cortical bone. It also uses a more sophisticated theoretical framework to

estimate structural and elastic parameters from both, cortical and trabecular bone compartments.

Theory and clinical applications of the two-wave phenomenon are described in detail in Chap. 6. Briefly, the system measures at the ultradistal radius region (see Fig. 6.16), at which the cortical shell is thin and the medullary cavity is filled with a dense trabecular network (Fig. 6.14). The device uses two coaxially and confocally aligned 1-MHz transducers (Fig. 3.4), which are mechanically scanned. Data are captured both, in transmission and pulse-echo modes. A coarse scan in transmission mode provides maps of apparent attenuation and sound velocity, which are used to select the scan region for the measurement of a direct wave through the radius (Fig. 6.17). Several bone properties are estimated from the combination of transmission and reflection measurements following the model described in Chap. 6. These include thickness of cortical bone (mm) (Mano et al., 2015), bone mass (bone mineral density (mg/cm^3)) and bone volume fraction BV/TV (%) of cancellous bone, and elastic constant of cancellous bone (GPa) (Otani, 2005). It should be noted that the estimations of these properties require the a priori knowledge of multiple properties. The estimation of cortical thickness is based on the analysis of time delays of outer and inner cortical boundaries measured in pulse-echo mode and conversion to thickness using the assumption of a constant

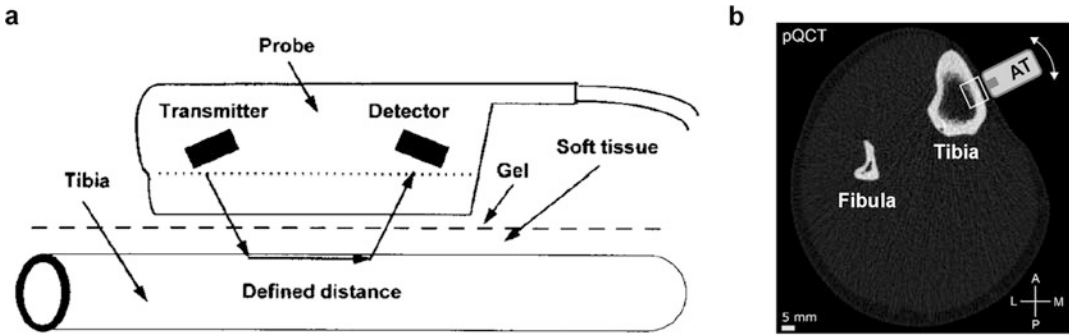


Fig. 3.5 Principle of cortical axial transmission (a), reprinted from Foldes et al. (1995) with permission. The measurements can be performed at tibia (b) and radius

bones, adapted and reprinted from Schneider et al. (2019) with permission

compression wave velocity in the radial direction of $c_p^{rad} = 3300$ m/s in cortical tissue:

$$Ct.Th = \frac{c_p^{rad} \cdot \Delta t}{2}. \quad (3.12)$$

A priori knowledge of propagation speeds, attenuation constants, densities and acoustic impedances of water, soft tissue and cortical bone are required for the estimations of the other parameters. However, as these properties are not known and can vary considerably, the properties reported by the device must be considered as “apparent” bone properties (Brebant et al., 2010). However, reasonable correlations with cortical thickness ($r = 0.88$) and cancellous bone density ($r = 0.76$) derived from high-resolution X-ray tomography have been obtained (see Figs. 16.18 and 16.19) and the system has been used successfully in different clinical studies (Sect. 16.3.2).

3.4 Cortical Axial Transmission

The principle of axial wave propagation differs considerably from conventional through-transmission and pulse-echo measurements (for a detailed description, see Chap. 4). These devices are designed to measure the propagation velocity of ultrasonic waves axially transmitted along cortical bone in long bones. The common

transducer arrangement for a cortical axial transmission measurement is shown in Fig. 3.5.

The SoundScan system was the first device introduced to measure the longitudinal transmission of an acoustic 250-kHz pulse along the cortical layer of the mid-tibia (Foldes et al., 1995). The probe is placed parallel to the longitudinal axis of the bone (Fig. 3.5a). The transducers are coupled to the skin through standard ultrasound gel. The transit time of a pulse along a defined 50-mm distance is measured. The probe is moved back and forth across the tibial surface and velocity readings are continuously recorded. The resultant velocity is an average of the five highest percent readings during the scan.

With the Omnisense, multi-site axial transmission was introduced commercially as the direct successor to tibial axial transmission. The device offers a family of small hand-held probes designed to measure various skeletal sites under different soft tissue thickness conditions. The smallest probes can be used to measure skeletal sites where the layer of covering soft tissue is the thinnest such as the finger phalanges, while the larger probes are dedicated for skeletal sites covered by a thicker layer of soft tissue such as the distal one-third radius. Still some patients cannot be measured due to thick soft tissue (Weiss et al., 2000). The main advantage of a multi-site device is the possibility of measuring skeletal sites which may be more relevant for fracture risk prediction than the tibia. While the basic measurement

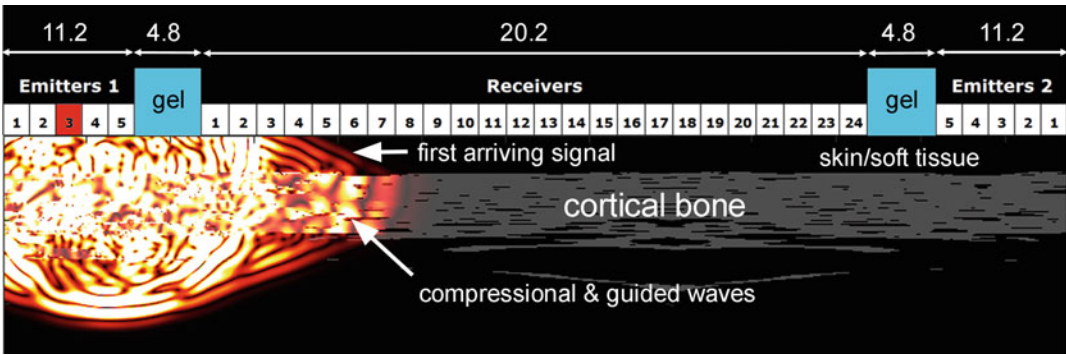


Fig. 3.6 Principle of bi-directional axial ultrasound transmission. The ultrasound transducer consists of two emitter arrays and one receiver array separated by gel filled gap regions (dimensions are given in mm). The numerical sound propagation simulation shows an ultrasound pulse emitted at element 3 of emitter array 1, which propagates through skin and soft tissue into the bone. One part of

the wave is transmitted into the medullary canal and other parts propagate as compressional and dispersive guided waves in the axial bone direction through the cortical shell. These waves leak acoustic waves back into the soft tissue which are detected by the central receiver array. (Reprinted from (Raimann et al., 2020) with permission)

principle is identical for all cortical axial transmission devices, the technical configurations and data analyses are quite different. The probe of the Omnisense device contains four 1.25-MHz transducers, i.e., a transducer pair and a receiver pair. The four ultrasonic transducers are used for an estimation of the velocity in the soft tissue between transducer and bone and to compensate changes in the tissue thickness along the bone. Moreover, to increase the amplitude of the transmitted and received signals, the transducers are mounted at an angle close to the critical angle relative to the surface of the probe. Both factors severely impact on the trueness of the “speed of sound” (SOS) measurement through bone. Although the exact algorithm used by the manufacturer remains undisclosed, one may reasonably assume that several ultrasonic recordings are performed by combining direct transmission or reflection between different transmitters and receivers, so that several acoustic pathways involving soft tissue path portions of the same length and variable bone path length may be analyzed. Thus, processing different signal propagation times yields the signal propagation velocity of the first arriving signal v_{FAS} . Depending on the thickness-to-wavelength ratio, different waves may be involved in the fastest part of the detected signal. Thereby, the reported SOS value may correspond to the velocity

of a bulk compression wave, a guided wave or a mixture of both (Raum et al., 2005).

The Sono device makes use of the excitation and analysis of a fundamental flexural guided wave (FFGW), which is equivalent to the lowest antisymmetric Lamb mode (i.e., A_0) for a plate (Moilanen et al., 2013). With the bi-directional axial transmission (BDAT) device an ultrasonic pulse is transmitted along the bone surface in two opposite directions from two sources placed at both ends of a distinct group of receivers (Fig. 3.6) (Bossy et al., 2004). A simple combination of the time delays derived from waves propagating in opposite directions efficiently corrects automatically for variable soft tissue thickness. In addition to the estimation of the first arriving signal the array configuration allows the full dispersion analysis of multiple dispersive waves by means of a 2-D spatio-temporal Fourier transform and dedicated signal processing (Minonzio et al., 2010). Different probes have been developed to ensure a suitable thickness-to-wavelength range for measurements with 1-MHz waves at the one-third distal radius (Minonzio et al., 2019; Vallet et al., 2016) and with 500-kHz waves at tibia bones (Schneider et al., 2019). In contrast to other bone QUS axial transmission devices, this method provides, under the assumptions that cortical bone behaves like a free wave-guiding isotropic plate

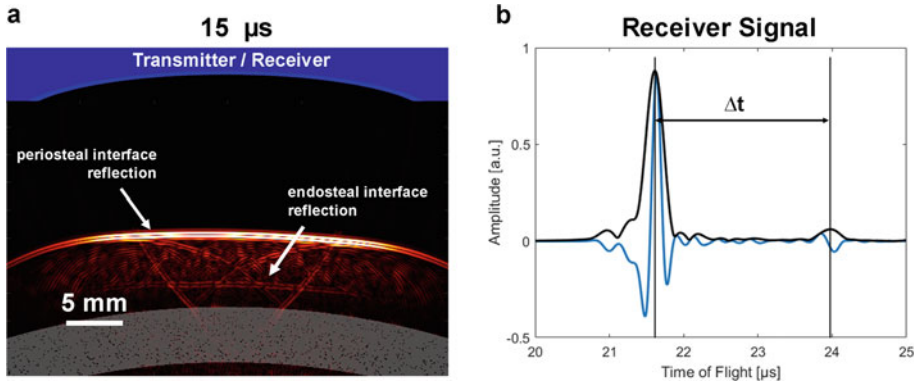


Fig. 3.7 Principle of pulse-echo measurement of the apparent cortical thickness (a) A single-element focused transducer emits a wave and receives signals reflected from the periosteal and endosteal cortical bone interfaces.

Pulse-echo signal and Hilbert-transformed envelope signal measured by the same transducer (b) The time delay Δt between these two reflections is converted to a thickness valued using the assumption of a constant sound velocity in the radial bone direction

and the tissue stiffness of the cortical bone is constant, real measurements of cortical porosity (Ct.Po) and cortical thickness (Ct.Th).

Other cortical axial transmission devices have been introduced but not yet commercialized, e.g., the dual frequency axial transmission (Tatarinov et al., 2014) and a low-frequency axial transmission (Vogl et al., 2019). The reader is referred to Chaps. 4 and 5 for a comprehensive introduction to the principles, signal processing and models implemented in this category of devices.

3.5 Cortical Pulse-Echo

Pulse-echo measurements using single-element transducers have been introduced by Karjalainen et al. (Karjalainen et al., 2012) and are now implemented in the Bindex device. This method provides estimates of the apparent cortical thickness Ct.Th measured at different anatomical sites, i.e., at proximal and distal tibia and at the distal radius. Moreover, a density index (DI) is calculated by a combination of age, weight, and multi-site apparent Ct.Th estimations. The device consists of a single-element focused transducer including a buffer-rod to send short ultrasound pulses through skin and soft tissue to the bone. If the beam inclination is approximately normal to the outer (periosteal) and inner (endosteal)

cortical bone interfaces, two reflections can be observed (Fig. 3.7a). The method relies on the assumptions that the specular reflections from periosteal and endosteal cortical bone interfaces are stronger than signals backscattered from cortical pores and that they are well separated in time, i.e., the time lag Δt between these two echoes can be measured using conventional peak detection algorithms applied to the envelope signal (Karjalainen et al., 2008) (see Fig. 3.7b). With the further assumption of a known and invariant radial sound velocity of $c_p^{rad} = 3565$ m/s, the apparent cortical thickness Ct.Th is derived via Eq. 3.12. This value was obtained in-vivo by comparison with site-matched peripheral computed tomography (pQCT, in-plane pixel size: $500 \mu\text{m} \times 500 \mu\text{m}$) on 20 young and healthy volunteers (12 males, age (mean \pm SD) 35.0 ± 12.7 years; 8 females, age (mean \pm SD) 42.1 ± 14.3 years) (Karjalainen et al., 2008). It should be noted that the center frequency of the probe used in that study was 2.25 MHz and that different c_p^{rad} values obtained at different measurement sites (proximal tibia: 3447 m/s; distal tibia: 3551 m/s; distal radius: 3634 m/s) were averaged. Accuracy and precision for the thickness estimation using the average value were reported to be 6.6% and 0.29 mm. This is in agreement with the reported error of 6% for Ct.Th by using use of a predefined, constant value for radial SOS (Eneh et al., 2016).

It was shown that the apparent cortical thickness measured at distal radius and distal tibia correlates with BMD ($r \geq 0.71$, $p < 0.001$, $0.30 < R^2 < 0.55$) (Behrens et al., 2016). Thereby, a density index (DI) was introduced in an in-vivo study on 30 elderly women (age: 74.4 ± 2.9 years) with and without hip fractures (Karjalainen et al., 2012). By means of multivariate linear regression using age, weight, and apparent Ct.Th measured at distal and proximal tibia a significant model with BMD measured at the neck ($r = 0.86$) was obtained. While these early proof-of-concept studies have used transducers with a center frequency of 2.25 MHz, the commercialized devices have a nominal center frequency of 3 MHz (Karjalainen et al., 2016, 2018; Schousboe et al., 2017).

3.6 Trabecular Pulse-Echo

In analogy to transmission measurements, trabecular bone can be probed in pulse-echo configuration. The implementation of radiofrequency echographic multi spectrometry (REMS) in a clinical device and the fundamentals of scattering in cancellous bone are covered in Chaps. 7 and 8, respectively. Briefly, the Echolight system uses conventional B-mode 128-element array technology including a 3.5 MHz convex transducer array (Casciaro et al., 2016) and sophisticated image processing and machine-learning based algorithms for automatically selecting the appropriate region of interest and for computing quantitative indices. Measurements are performed at the spine (through the abdomen) or at the femoral neck. An “Osteoporosis Score” OS is derived by comparison of the mean power spectrum measured in a patient with age-, sex-, BMI- and site-matched spectral models of pathologic and healthy conditions, which were derived empirically by comparison with DXA-based BMD values (Casciaro et al., 2016). Similarly, the “Fragility Score” is obtained by comparing an analogous spectral similarity to subjects that reported a recent fragility fracture with respect to control subjects without fracture history (see Chap. 7 for further details). Although

the methods are not ground on a physical backscatter model, reasonable predictions of BMD have been obtained in postmenopausal women ($R = 0.87$) (Casciaro et al., 2016).

3.7 What Has Been Achieved and What Is Still Missing in Bone QUS?

Years 1990–2000 have been the decade of the QUS golden age with heel transverse transmission measuring BUA and SOS. A few heel devices such as the Achilles (GE Healthcare) and the Sahara (Hologic) were validated through large scale prospective studies including tens of thousands of patients. However, despite good clinical performances and a general clinical consensus that they were useful for fracture risk assessment and case-finding, particularly in regions of the world where access to DXA is uneasy (see Chap. 2), these approaches have generally declined and receded in the background. The low added value and the lack of standardization compared to DXA as well as the missing therapeutic trials with QUS-based inclusion of patients have been major obstacles to the broader establishment of heel transverse transmission in clinical routine. Currently, DXA remains the main modality used for the clinical management of osteoporotic patients and in addition to heel ultrasound a variety of other QUS modalities have been established, which provide bone density surrogate markers (e.g., BMD_{US} Density Index, T- and Z-scores) derived from empirical correlations with BMD. Meanwhile, with the development of high-resolution peripheral computed tomography a focus has been placed on the key role played by cortical bone in bone strength and on the importance of assessing cortical bone for a better clinical management of osteoporotic patients (Zebaze et al., 2010). This has revitalized the research effort on cortical bone quantitative ultrasound and years 2010–2020 have seen a major surge in the development and clinical application of technologies for the assessment of cortical bone, including developments of axial transmission, scattering, pulse-echo techniques and imaging methods. Al-

though most of the modern QUS approaches have been developed for the application at peripheral skeletal sites for practical reasons, e.g., ease of access and minimal influence of soft tissue, these measurement sites have now been confirmed to be highly relevant for the identification people at high risk for fragility fractures at the spine and other skeletal sites. For example, decreased cortical thickness and the prevalence of large BMU's at the tibia have been shown *ex-vivo* to be quantifiable 'fingerprints' of structural deterioration at the femoral neck (Iori et al., 2020) and reduced proximal femur bone strength (Iori et al., 2019). While some of the recent technologies (e.g., BI and LD-100) assess an "apparent thickness", a model-based measurement cortical thickness and cortical porosity Ct.Po has been achieved for the first time with the BDAT system by means of multimode waveguide dispersion analysis in axial transmission measurements. The method considers variations of porosity as a major source of variations of cortical bone elasticity, sound velocity and compression strength in postmenopausal women (Granke et al., 2011; Granke et al., 2016; Peralta et al., 2021). Results of a first validation study in postmenopausal women confirmed a comparable fracture discrimination performance of the BDAT variables as BMD for both vertebral and peripheral fractures (see Chap. 4). However, axial transmission measurements do not provide direct image-guidance and are restricted to patients with low BMI (Minonzio et al., 2019).

In contrast to other bone QUS devices, Echolight has introduced the first bone QUS system based on a conventional medical ultrasound pulse-echo imaging platform. Moreover, they target with their approach the two major fracture sites, i.e., hip and spine (see Chap. 7). As ultrasound scanners are the by far most frequently applied imaging devices in clinical routine, the approach has great potential to reach a widespread application if it can be integrated into existing or future scanners from various vendors. The measurements are conducted through thick layers of soft tissue. However, as the REMS technology provides only ultrasound-based BMD surrogate parameters and empirical associations with the occurrence of fragility

fractures, the technology may provide a non-ionizing diagnostic alternative to the DXA measurement but cannot surpass the limitations of BMD for the identification of people with increased fracture risk despite non-osteoporotic BMD values.

Other promising technologies with a potential to complement or even surpass current radiative gold standards are still under development. These methods benefit from the increasing availability of sophisticated open programmable ultrasound platforms with multichannel data acquisition hardware. With these systems, the Delay-And-Sum (DAS) beamforming integrated into the hardware of conventional medical ultrasound scanners to reconstruct images from the ultrasound backscattered signals can be overcome. Thereby, the strong distortions of acoustic waves caused by refraction, scattering and diffusion at bone-soft tissue boundaries and intracortical pores can be incorporated in the image reconstruction. One promising recent research direction combines pulse-echo imaging using conventional medical ultrasound array imaging technology with refraction corrected multifocal image reconstruction (Nguyen Minh et al., 2020). The algorithm provides local estimations of both cortical thickness and sound velocity. Another sophisticated inversion method was inspired from seismic image reconstruction to image the internal structure (i.e., the endosteal cortical bone interface) of long bones (Renaud et al., 2018). This reconstruction algorithm also provides local estimations of Ct.Th and anisotropic sound velocity, and can even assess intraosseous blood perfusion (see Chap. 10).

The diversity by which ultrasound interactions with cortical bone are explored are still expanding. For example, multiple scattering and sound diffusion models hold the possibility to assess cortical bone properties, such as pore size and density (Karbalaiesadegh et al., 2019) from backscattered waves (see Chap. 9). Very recently, Iori et al. (Iori et al., 2021) have proposed a cortical bone backscatter model, from which, for the first time, the cortical pore size distribution in the range between 20 and 120 μm could be retrieved (Iori et al., 2021).

It should be noted that this pore size range is not resolvable by any other medical imaging modality but covers the transition from normal to pathologically increased pore dimensions. In the ex-vivo study, pore structure, particularly the parameters describing prevalence of large pores could be predicted with high accuracy (adj. $R^2 \geq 0.54$). The combination of cortical thickness and backscatter parameters measured at the tibia were highly associated with stiffness and ultimate force of the proximal femur (adj. $R^2 \geq 0.54$). When combined with cortical thickness, 78% of the variation of the ultimate force at the proximal femur could be explained.

So far, these novel cortical bone imaging methods have been developed and validated in-silico, ex-vivo on a few healthy volunteers, or in small pilot studies. In a first pilot study on 55 postmenopausal women with low BMD (Armbrecht et al., 2021), cortical pore size distribution and frequency-dependent attenuation assessed from cortical bone backscatter measurements demonstrated superior discrimination performance for fragility fractures (area under the receiver operating characteristic curve [AUC]: $0.69 \leq \text{AUC} \leq 0.75$) compared with DXA ($0.54 \leq \text{AUC} \leq 0.55$). Their potential for the diagnosis of osteoporosis and fracture risk prediction has yet to be demonstrated in clinical studies.

References

- Adami, G., Arioli, G., Bianchi, G., Brandi, M. L., Caffarelli, C., Cianferotti, L., Gatti, D., Girasole, G., Gonnelli, S., Manfredini, M., et al. (2020). Radiofrequency echographic multi spectrometry for the prediction of incident fragility fractures: A 5-year follow-up study. *Bone*, *134*, 115297.
- Alenfeld, F. E., Engelke, K., Schmidt, D., Brezger, M., Diessel, E., & Felsenberg, D. (2002). Diagnostic agreement of two calcaneal ultrasound devices: The Sahara bone sonometer and the Achilles+. *The British Journal of Radiology*, *75*, 895–902.
- Anderson, C. C., Marutyan, K. R., Holland, M. R., Wear, K. A., & Miller, J. G. (2008). Interference between wave modes may contribute to the apparent negative dispersion observed in cancellous bone. *The Journal of the Acoustical Society of America*, *124*, 1781–1789.
- Armbrecht, G., Nguyen Minh, H., Massmann, J., & Raum, K. (2021). Pore-size distribution and frequency-dependent attenuation in human cortical tibia bone discriminate fragility fractures in postmenopausal women with low bone mineral density. *JBMRplus*, *5*(11), e10536. <https://pubmed.ncbi.nlm.nih.gov/34761144/>
- Bala, Y., Zebaze, R., Ghasem-Zadeh, A., Atkinson, E. J., Iuliano, S., Peterson, J. M., Amin, S., Bjornerem, A., Melton, L. J., 3rd, Johansson, H., et al. (2014). Cortical porosity identifies women with osteopenia at increased risk for forearm fractures. *Journal of Bone and Mineral Research*, *29*, 1356–1362.
- Barkmann, R., Laugier, P., Moser, U., Dencks, S., Klausner, M., Padilla, F., Haiat, G., Heller, M., & Gluer, C. C. (2008). In vivo measurements of ultrasound transmission through the human proximal femur. *Ultrasound in Medicine & Biology*, *34*, 1186–1190.
- Barkmann, R., Dencks, S., Laugier, P., Padilla, F., Brixen, K., Ryg, J., Seekamp, A., Mahlke, L., Bremer, A., Heller, M., et al. (2010). Femur ultrasound (FemUS)—first clinical results on hip fracture discrimination and estimation of femoral BMD. *Osteoporosis International*, *21*, 969–976.
- Bauer, A. Q., Marutyan, K. R., Holland, M. R., & Miller, J. G. (2008). Negative dispersion in bone: The role of interference in measurements of the apparent phase velocity of two temporally overlapping signals. *The Journal of the Acoustical Society of America*, *123*, 2407–2414.
- Behrens, M., Felser, S., Mau-Moeller, A., Weippert, M., Pollex, J., Skripitz, R., Herlyn, P. K., Fischer, D. C., Bruhn, S., Schober, H. C., et al. (2016). The Bindex(R) ultrasound device: Reliability of cortical bone thickness measures and their relationship to regional bone mineral density. *Physiological Measurement*, *37*, 1528–1540.
- Bjornerem, A., Bui, Q. M., Ghasem-Zadeh, A., Hopper, J. L., Zebaze, R., & Seeman, E. (2013). Fracture risk and height: An association partly accounted for by cortical porosity of relatively thinner cortices. *Journal of Bone and Mineral Research*, *28*, 2017–2026.
- Bossy, E., Talmant, M., & Laugier, P. (2002). Effect of bone cortical thickness on velocity measurements using ultrasonic axial transmission: A 2D simulation study. *The Journal of the Acoustical Society of America*, *112*, 297–307.
- Bossy, E., Talmant, M., Defontaine, M., Patat, F., & Laugier, P. (2004). Bidirectional axial transmission can improve accuracy and precision of ultrasonic velocity measurement in cortical bone: A validation on test materials. *IEEE Transactions on Ultrasonics, Ferroelectrics, and Frequency Control*, *51*, 71–79.
- Bouxsein, M. L., Coan, B. S., & Lee, S. C. (1999). Prediction of the strength of the elderly proximal femur by bone mineral density and quantitative ultrasound measurements of the heel and tibia. *Bone*, *25*, 49–54.
- Breban, S., Padilla, F., Fujisawa, Y., Mano, I., Matsukawa, M., Benhamou, C. L., Otani, T., Laugier, P., & Chapard, C. (2010). Trabecular and cortical bone separately assessed at radius with a new ultrasound device, in a young adult population with various physical activities. *Bone*, *46*, 1620–1625.

- Casciaro, S., Peccarisi, M., Pisani, P., Franchini, R., Greco, A., De Marco, T., Grimaldi, A., Quarta, L., Quarta, E., Muratore, M., et al. (2016). An advanced quantitative Echostore methodology for femoral neck densitometry. *Ultrasound in Medicine & Biology*, *42*, 1337–1356.
- Chaffai, S., Padilla, F., Berger, G., & Laugier, P. (2000). In vitro measurement of the frequency-dependent attenuation in cancellous bone between 0.2 and 2 MHz. *The Journal of the Acoustical Society of America*, *108*, 1281–1289.
- Chan, M. Y., Nguyen, N. D., Center, J. R., Eisman, J. A., & Nguyen, T. V. (2013). Quantitative ultrasound and fracture risk prediction in non-osteoporotic men and women as defined by WHO criteria. *Osteoporosis International*, *24*, 1015–1022.
- Chappard, C., Laugier, P., Fournier, B., Roux, C., & Berger, G. (1997). Assessment of the relationship between broadband ultrasound attenuation and bone mineral density at the calcaneus using BUA imaging and DXA. *Osteoporosis International*, *7*, 316–322.
- Delshad, M., Beck, K. L., Conlon, C. A., Mugridge, O., Kruger, M. C., & von Hurst, P. R. (2020). Validity of quantitative ultrasound and bioelectrical impedance analysis for measuring bone density and body composition in children. *European Journal of Clinical Nutrition*, *75*, 66–72.
- Di Paola, M., Gatti, D., Viapiana, O., Cianferotti, L., Cavalli, L., Caffarelli, C., Conversano, F., Quarta, E., Pisani, P., Girasole, G., et al. (2019). Radiofrequency echographic multispectrometry compared with dual X-ray absorptiometry for osteoporosis diagnosis on lumbar spine and femoral neck. *Osteoporosis International*, *30*, 391–402.
- Diez-Perez, A., Brandi, M. L., Al-Daghri, N., Branco, J. C., Bruyere, O., Cavalli, L., Cooper, C., Cortet, B., Dawson-Hughes, B., Dimai, H. P., et al. (2019). Radiofrequency echographic multi-spectrometry for the in-vivo assessment of bone strength: State of the art-outcomes of an expert consensus meeting organized by the European Society for Clinical and Economic Aspects of Osteoporosis, Osteoarthritis and Musculoskeletal Diseases (ESCEO). *Aging Clinical and Experimental Research*, *31*, 1375–1389.
- Dobnig, H., Pitswanger-Solkner, J. C., Obermayer-Pietsch, B., Tiran, A., Strele, A., Maier, E., Maritschnegg, P., Riedmuller, G., Brueck, C., & Fahrleitner-Pammer, A. (2007). Hip and nonvertebral fracture prediction in nursing home patients: Role of bone ultrasound and bone marker measurements. *The Journal of Clinical Endocrinology and Metabolism*, *92*, 1678–1686.
- Droin, P., Berger, G., & Laugier, P. (1998). Velocity dispersion of acoustic waves in cancellous bone. *IEEE Transactions on Ultrasonics, Ferroelectrics, and Frequency Control*, *45*, 581–592.
- Eneh, C. T., Malo, M. K., Karjalainen, J. P., Liukkonen, J., Toyras, J., & Jurvelin, J. S. (2016). Effect of porosity, tissue density, and mechanical properties on radial sound speed in human cortical bone. *Medical Physics*, *43*, 2030.
- Foldes, A. J., Rimon, A., Keinan, D. D., & Popovtzer, M. M. (1995). Quantitative ultrasound of the tibia: A novel approach for assessment of bone status. *Bone*, *17*, 363–367.
- Gluer, C. C., Eastell, R., Reid, D. M., Felsenberg, D., Roux, C., Barkmann, R., Timm, W., Blenk, T., Armbrrecht, G., Stewart, A., et al. (2004). Association of five quantitative ultrasound devices and bone densitometry with osteoporotic vertebral fractures in a population-based sample: The OPUS Study. *Journal of Bone and Mineral Research*, *19*, 782–793.
- Gonnelli, S., Cepollaro, C., Gennari, L., Montagnani, A., Caffarelli, C., Merlotti, D., Rossi, S., Cadimi, A., & Nuti, R. (2005). Quantitative ultrasound and dual-energy X-ray absorptiometry in the prediction of fragility fracture in men. *Osteoporosis International*, *16*, 963–968.
- Granke, M., Grimal, Q., Saied, A., Nauleau, P., Peyrin, F., & Laugier, P. (2011). Change in porosity is the major determinant of the variation of cortical bone elasticity at the millimeter scale in aged women. *Bone*, *49*, 1020–1026.
- Granke, M., Makowski, A. J., Uppuganti, S., & Nyman, J. S. (2016). Prevalent role of porosity and osteonal area over mineralization heterogeneity in the fracture toughness of human cortical bone. *Journal of Biomechanics*, *49*, 2748–2755.
- Hans, D., Schott, A. M., Chapuy, M. C., Benamar, M., Kotzki, P. D., Cormier, C., Pouilles, J. M., & Meunier, P. J. (1994). Ultrasound measurements on the os calcis in a prospective multicenter study. *Calcified Tissue International*, *55*, 94–99.
- He, Y. Q., Fan, B., Hans, D., Li, J., Wu, C. Y., Njeh, C. F., Zhao, S., Lu, Y., Tsuda-Futami, E., Fuerst, T., et al. (2000). Assessment of a new quantitative ultrasound calcaneus measurement: Precision and discrimination of hip fractures in elderly women compared with dual X-ray absorptiometry. *Osteoporosis International*, *11*, 354–360.
- Ingle, B. M., Sherwood, K. E., & Eastell, R. (2001). Comparison of two methods for measuring ultrasound properties of the heel in postmenopausal women. *Osteoporosis International*, *12*, 500–505.
- Iori, G., Schneider, J., Reisinger, A., Heyer, F., Peralta, L., Wyers, C., Grasel, M., Barkmann, R., Gluer, C. C., van den Bergh, J. P., et al. (2019). Large cortical bone pores in the tibia are associated with proximal femur strength. *PLoS One*, *14*, e0215405.
- Iori, G., Schneider, J., Reisinger, A., Heyer, F., Peralta, L., Wyers, C., Gluer, C. C., van den Bergh, J. P., Pahr, D., & Raum, K. (2020). Cortical thinning and accumulation of large cortical pores in the tibia reflect local structural deterioration of the femoral neck. *Bone*, *137*, 115446.
- Iori, G., Du, J., Hackenbeck, J., Kilappa, V., & Raum, K. (2021). Estimation of cortical bone microstructure from ultrasound backscatter. *IEEE Transactions on Ultrasonics, Ferroelectrics, and Frequency Control*, *68*, 1081–1095.
- Jafri, L., Majid, H., Ahmed, S., Naureen, G., & Khan, A. H. (2020). Calcaneal ultrasound and its relation to di-

- etary and lifestyle factors, anthropometry, and Vitamin D deficiency in Young medical students. *Frontiers in Endocrinology (Lausanne)*, 11, 601562.
- Karbalaeisadegh, Y., Yousefian, O., Iori, G., Raum, K., & Muller, M. (2019). Acoustic diffusion constant of cortical bone: Numerical simulation study of the effect of pore size and pore density on multiple scattering. *The Journal of the Acoustical Society of America*, 146, 1015.
- Karjalainen, J., Riekkinen, O., Toyras, J., Kroger, H., & Jurvelin, J. (2008). Ultrasonic assessment of cortical bone thickness in vitro and in vivo. *IEEE Transactions on Ultrasonics, Ferroelectrics, and Frequency Control*, 55, 2191–2197.
- Karjalainen, J. P., Riekkinen, O., Toyras, J., Hakulinen, M., Kroger, H., Rikkonen, T., Salovaara, K., & Jurvelin, J. S. (2012). Multi-site bone ultrasound measurements in elderly women with and without previous hip fractures. *Osteoporosis International*, 23, 1287–1295.
- Karjalainen, J. P., Riekkinen, O., Toyras, J., Jurvelin, J. S., & Kroger, H. (2016). New method for point-of-care osteoporosis screening and diagnostics. *Osteoporosis International*, 27, 971–977.
- Karjalainen, J. P., Riekkinen, O., & Kroger, H. (2018). Pulse-echo ultrasound method for detection of postmenopausal women with osteoporotic BMD. *Osteoporosis International*, 29, 1193–1199.
- Kazakia, G. J., Nirody, J. A., Bernstein, G., Sode, M., Burghardt, A. J., & Majumdar, S. (2013). Age- and gender-related differences in cortical geometry and microstructure: Improved sensitivity by regional analysis. *Bone*, 52, 623–631.
- Krieg, M. A., Barkmann, R., Gonnelli, S., Stewart, A., Bauer, D. C., Del Rio Barquero, L., Kaufman, J. J., Lorenc, R., Miller, P. D., Olszynski, W. P., et al. (2008). Quantitative ultrasound in the management of osteoporosis: The 2007 ISCD official positions. *Journal of Clinical Densitometry*, 11, 163–187.
- Lam, T. P., Hung, V. W., Yeung, H. Y., Tse, Y. K., Chu, W. C., Ng, B. K., Lee, K. M., Qin, L., & Cheng, J. C. (2011). Abnormal bone quality in adolescent idiopathic scoliosis: A case-control study on 635 subjects and 269 normal controls with bone densitometry and quantitative ultrasound. *Spine (Phila Pa 1976)*, 36, 1211–1217.
- Langton, C. M., Palmer, S. B., & Porter, R. W. (1984). The measurement of broadband ultrasonic attenuation in cancellous bone. *Engineering in Medicine*, 13, 89–91.
- Laugier, P. (2008). Instrumentation for in vivo ultrasonic characterization of bone strength. *IEEE Transactions on Ultrasonics, Ferroelectrics, and Frequency Control*, 55, 1179–1196.
- Laugier, P., Droin, P., Laval-Jeantet, A. M., & Berger, G. (1997). In vitro assessment of the relationship between acoustic properties and bone mass density of the calcaneus by comparison of ultrasound parametric imaging and quantitative computed tomography. *Bone*, 20, 157–165.
- Le Floch, V., Luo, G., Kaufman, J. J., & Siffert, R. S. (2008). Ultrasonic assessment of the radius in vitro. *Ultrasound in Medicine & Biology*, 34, 1972–1979.
- Lewiecki, E. M. (2020). Pulse-echo ultrasound identifies Caucasian and Hispanic women at risk for osteoporosis. *Journal of Clinical Densitometry*, 24(2), 175–182.
- Liu, C., Li, B., Li, Y., Mao, W., Chen, C., Zhang, R., & Ta, D. (2020). Ultrasonic backscatter difference measurement of bone health in preterm and term newborns. *Ultrasound in Medicine & Biology*, 46, 305–314.
- Mano, I., Horii, K., Hagino, H., Miki, T., Matsukawa, M., & Otani, T. (2015). Estimation of in vivo cortical bone thickness using ultrasonic waves. *Journal of Medical Ultrasonics*, 2001(42), 315–322.
- Mao, W. Y., Du, Y., Liu, C. C., Li, B. Y., Ta, D. A., Chen, C., & Zhang, R. (2019). Ultrasonic backscatter technique for assessing and monitoring neonatal cancellous bone status in vivo. *IEEE Access*, 7, 157417–157426.
- Marin, F., Gonzalez-Macias, J., Diez-Perez, A., Palma, S., & Delgado-Rodriguez, M. (2006). Relationship between bone quantitative ultrasound and fractures: A meta-analysis. *Journal of Bone and Mineral Research*, 21, 1126–1135.
- Miller, P. D., Siris, E. S., Barrett-Connor, E., Faulkner, K. G., Wehren, L. E., Abbott, T. A., Chen, Y. T., Berger, M. L., Santora, A. C., & Sherwood, L. M. (2002). Prediction of fracture risk in postmenopausal white women with peripheral bone densitometry: Evidence from the National Osteoporosis Risk Assessment. *Journal of Bone and Mineral Research*, 17, 2222–2230.
- Minonzio, J. G., Talmant, M., & Laugier, P. (2010). Guided wave phase velocity measurement using multi-emitter and multi-receiver arrays in the axial transmission configuration. *The Journal of the Acoustical Society of America*, 127, 2913–2919.
- Minonzio, J. G., Bochud, N., Vallet, Q., Ramiandrisoa, D., Etcheto, A., Briot, K., Kolta, S., Roux, C., & Laugier, P. (2019). Ultrasound-based estimates of cortical bone thickness and porosity are associated with nontraumatic fractures in postmenopausal women: A pilot study. *Journal of Bone and Mineral Research*, 34, 1585–1596.
- Moayeri, A., Kaptoge, S., Dalzell, N., Bingham, S., Luben, R. N., Wareham, N. J., Reeve, J., & Khaw, K. T. (2009). Is QUS or DXA better for predicting the 10-year absolute risk of fracture? *Journal of Bone and Mineral Research*, 24, 1319–1325.
- Moilanen, P., Maatta, M., Kilappa, V., Xu, L., Nicholson, P. H., Alen, M., Timonen, J., Jamsa, T., & Cheng, S. (2013). Discrimination of fractures by low-frequency axial transmission ultrasound in postmenopausal females. *Osteoporosis International*, 24, 723–730.
- Nazari-Farsani, S., Vuopio, M. E., & Aro, H. T. (2020). Bone mineral density and cortical-bone thickness of the distal radius predict femoral stem subsidence in postmenopausal women. *The Journal of Arthroplasty*, 35(1877–1884), e1871.
- Nguyen Minh, H., Du, J., & Raum, K. (2020). Estimation of thickness and speed of sound in cortical bone using multifocus pulse-Echo ultrasound. *IEEE Transactions*

- on *Ultrasonics, Ferroelectrics, and Frequency Control*, 67, 568–579.
- Nicholson, P. H., Lowet, G., Langton, C. M., Dequeker, J., & Van der Perre, G. (1996). A comparison of time-domain and frequency-domain approaches to ultrasonic velocity measurement in trabecular bone. *Physics in Medicine and Biology*, 41, 2421–2435.
- Nicholson, J. A., Yapp, L. Z., Keating, J. F., & Simpson, A. (2020). Monitoring of fracture healing. Update on current and future imaging modalities to predict union. *Injury*, 52, S29–S34.
- Njeh, C. F., Hans, D., Li, J., Fan, B., Fuerst, T., He, Y. Q., Tsuda-Futami, E., Lu, Y., Wu, C. Y., & Genant, H. K. (2000). Comparison of six calcaneal quantitative ultrasound devices: Precision and hip fracture discrimination. *Osteoporosis International*, 11, 1051–1062.
- Olmos, J. M., Hernandez, J. L., Pariente, E., Martinez, J., Valero, C., & Gonzalez-Macias, J. (2020). Trabecular bone score and bone quantitative ultrasound in Spanish postmenopausal women. *The Camargo Cohort Study. Maturitas*, 132, 24–29.
- Otani, T. (2005). Quantitative estimation of bone density and bone quality using acoustic parameters of cancellous bone for fast and slow waves. *Japanese Journal of Applied Physics*, 1(44), 4578–4582.
- Peralta, L., Maeztu Redin, J. D., Fan, F., Cai, X., Laugier, P., Schneider, J., Raum, K., & Grimal, Q. (2021). Bulk wave velocities in cortical bone reflect porosity and compression strength. *Ultrasound in Medicine & Biology*, 47, 799–808.
- Raimann, A., Mehany, S. N., Feil, P., Weber, M., Pietschmann, P., Boni-Mikats, A., Klepochova, R., Krssak, M., Hausler, G., Schneider, J., et al. (2020). Decreased compressional sound velocity is an indicator for compromised bone stiffness in X-linked Hypophosphatemic rickets (XLH). *Frontiers in Endocrinology (Lausanne)*, 11, 355.
- Ramteke, S. M., Kaufman, J. J., Arpadi, S. M., Shiau, S., Strehlau, R., Patel, F., Mbete, N., Coovadia, A., & Yin, M. T. (2017). Unusually high calcaneal speed of sound measurements in children with small foot size. *Ultrasound in Medicine & Biology*, 43, 357–361.
- Raum, K., Leguerey, I., Chandelier, F., Bossy, E., Talmant, M., Saied, A., Peyrin, F., & Laugier, P. (2005). Bone microstructure and elastic tissue properties are reflected in QUS axial transmission measurements. *Ultrasound in Medicine & Biology*, 31, 1225–1235.
- Renaud, G., Kruizinga, P., Cassereau, D., & Laugier, P. (2018). In vivo ultrasound imaging of the bone cortex. *Physics in Medicine and Biology*, 63, 125010.
- Roggen, I., Louis, O., Van Biervliet, S., Van Daele, S., Robberecht, E., De Wachter, E., Malfroot, A., De Waele, K., Gies, I., Vanbesien, J., et al. (2015). Quantitative bone ultrasound at the distal radius in adults with cystic fibrosis. *Ultrasound in Medicine & Biology*, 41, 334–338.
- Sakata, S., Barkmann, R., Lochmuller, E. M., Heller, M., & Gluer, C. C. (2004). Assessing bone status beyond BMD: Evaluation of bone geometry and porosity by quantitative ultrasound of human finger phalanges. *Journal of Bone and Mineral Research*, 19, 924–930.
- Sasagawa, M., Hasegawa, T., Kazama, J. J., Koya, T., Sakagami, T., Suzuki, K., Hara, K., Satoh, H., Fujimori, K., Yoshimine, F., et al. (2011). Assessment of bone status in inhaled corticosteroid user asthmatic patients with an ultrasound measurement method. *Allergology International*, 60, 459–465.
- Savino, F., Viola, S., Benetti, S., Ceratto, S., Tarasco, V., Lupica, M. M., & Cordero di Montezemolo, L. (2013). Quantitative ultrasound applied to metacarpal bone in infants. *PeerJ*, 1, e141.
- Schneider, J., Ramiandrisoa, D., Ambrecht, G., Ritter, Z., Felsenberg, D., Raum, K., & Minonzio, J. G. (2019). In vivo measurements of cortical thickness and porosity at the proximal third of the tibia using guided waves: Comparison with site-matched peripheral quantitative computed tomography and distal high-resolution peripheral quantitative computed tomography. *Ultrasound in Medicine & Biology*, 45, 1234–1242.
- Schousboe, J. T., Riekkinen, O., & Karjalainen, J. (2017). Prediction of hip osteoporosis by DXA using a novel pulse-echo ultrasound device. *Osteoporosis International*, 28, 85–93.
- Shenoy, S., Chawla, J. K., Gupta, S., & Sandhu, J. S. (2017). Prevalence of low bone health using quantitative ultrasound in Indian women aged 41–60 years: Its association with nutrition and other related risk factors. *Journal of Women & Aging*, 29, 334–347.
- Siegel, I. M., Anast, G. T., & Fields, T. (1958). The determination of fracture healing by measurement of sound velocity across the fracture site. *Surgery, Gynecology & Obstetrics*, 107, 327–332.
- Stein, E. M., Rosete, F., Young, P., Kamanda-Kosseh, M., McMahon, D. J., Luo, G., Kaufman, J. J., Shane, E., & Siffert, R. S. (2013). Clinical assessment of the 1/3 radius using a new desktop ultrasonic bone densitometer. *Ultrasound in Medicine & Biology*, 39, 388–395.
- Strelitzki, R., & Evans, J. A. (1998). Diffraction and interface losses in broadband ultrasound attenuation measurements of the calcaneum. *Physiological Measurement*, 19, 197–204.
- Strelitzki, R., Clarke, A. J., & Evans, J. A. (1996). The measurement of the velocity of ultrasound in fixed trabecular bone using broadband pulses and single-frequency tone bursts. *Physics in Medicine and Biology*, 41, 743–753.
- Tatarinov, A., Egorov, V., Sarvazyan, N., & Sarvazyan, A. (2014). Multi-frequency axial transmission bone ultrasonometer. *Ultrasonics*, 54, 1162–1169.
- To, W. W., & Wong, M. W. (2011). Bone mineral density changes in pregnancies with gestational hypertension: A longitudinal study using quantitative ultrasound measurements. *Archives of Gynecology and Obstetrics*, 284, 39–44.
- Tsuda-Futami, E., Hans, D., Njeh, C. F., Fuerst, T., Fan, B., Li, J., He, Y. Q., & Genant, H. K. (1999). An evaluation of a new gel-coupled ultrasound device for

- the quantitative assessment of bone. *The British Journal of Radiology*, 72, 691–700.
- Vallet, Q., Bochud, N., Chappard, C., Laugier, P., & Minonizio, J. G. (2016). In vivo characterization of cortical bone using guided waves measured by axial transmission. *IEEE Transactions on Ultrasonics, Ferroelectrics, and Frequency Control*, 63, 1361–1371.
- van den Berg, P., Schweitzer, D. H., van Haard, P. M. M., Geusens, P. P., & van den Bergh, J. P. (2020). The use of pulse-echo ultrasound in women with a recent non-vertebral fracture to identify those without osteoporosis and/or a subclinical vertebral fracture: A pilot study. *Archives of Osteoporosis*, 15, 56.
- Vogl, F., Patil, M., & Taylor, W. R. (2019). Sensitivity of low-frequency axial transmission acoustics to axially and azimuthally varying cortical thickness: A phantom-based study. *PLoS One*, 14, e0219360.
- Wear, K. A. (2000). The effects of frequency-dependent attenuation and dispersion on sound speed measurements: Applications in human trabecular bone. *IEEE Transactions on Ultrasonics, Ferroelectrics, and Frequency Control*, 47, 265–273.
- Wear, K. A. (2001). Ultrasonic attenuation in human calcaneus from 0.2 to 1.7 MHz. *IEEE Transactions on Ultrasonics, Ferroelectrics, and Frequency Control*, 48, 602–608.
- Wear, K. A. (2008). A method for improved standardization of in vivo calcaneal time-domain speed-of-sound measurements. *IEEE Transactions on Ultrasonics, Ferroelectrics, and Frequency Control*, 55, 1473–1479.
- Weiss, M., Ben-Shlomo, A., Hagag, P., & Ish-Shalom, S. (2000). Discrimination of proximal hip fracture by quantitative ultrasound measurement at the radius. *Osteoporosis International*, 11, 411–416.
- Wong, Y. S., Lai, K. K., Zheng, Y. P., Wong, L. L., Ng, B. K., Hung, A. L., Yip, B. H., Chu, W. C., Ng, A. W., Qiu, Y., et al. (2019). Is radiation-free ultrasound accurate for quantitative assessment of spinal deformity in idiopathic scoliosis (IS): A detailed analysis with EOS radiography on 952 patients. *Ultrasound in Medicine & Biology*, 45, 2866–2877.
- Xu, W., & Kaufman, J. J. (1993). Diffraction correction methods for insertion ultrasound attenuation estimation. *IEEE Transactions on Biomedical Engineering*, 40, 563–570.
- Zebaze, R. M., Ghasem-Zadeh, A., Bohte, A., Iuliano-Burns, S., Mirams, M., Price, R. I., Mackie, E. J., & Seeman, E. (2010). Intracortical remodelling and porosity in the distal radius and post-mortem femurs of women: A cross-sectional study. *Lancet*, 375, 1729–1736.